



<https://technobius.kz/>

e-ISSN  
3007-0147

# Technobius Physics

*A peer-reviewed open-access journal*

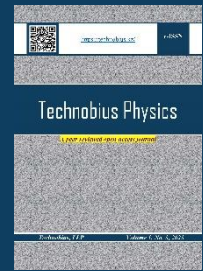
*Technobius, LLP*

*Volume 1, No. 4, 2023*



# Technobius Physics

Volume 1, No. 4, 2023



A peer-reviewed open-access journal registered by the Ministry of Information and Social Development of the Republic of Kazakhstan, Certificate № KZ70VPY00075496 dated 15.08.2023

**ISSN (Online):** 3007-0147

**Thematic Directions:** General Physics, Condensed Matter Physics

**Publisher:** Technobius, LLP

**Address:** 2 Turkestan street, office 116, 010000, Astana, Republic of Kazakhstan

**Editor-in-Chief:**

   *Aida Nazarova*, PhD, Laboratory Assistant, Department of Physics, Nazarbayev University, Astana, Kazakhstan

**Technical Editor:**

   *Saeed Nasiri*, Dr, Professor, Department of Physics, Nazarbayev University, Astana, Kazakhstan

**Editors:**

-   *Sang Ma Lee*, Dr., Professor, Engineering Research Center for Net Shape and Die Manufacturing, Pusan National University, Busan, South Korea
-   *Suk Bong Kang*, Dr., Professor, Korea Institute of Materials Science, Changwon, South Korea
-   *Marshall Onellion*, Dr., Professor, Department of Physics, University of Wisconsin-Madison, Madison, United States
-    *Bill Wheatle*, Dr, Assistant Professor, McKetta Department of Chemical Engineering, The University of Texas at Austin, Austin, United States
-   *Hyun-ho Kim*, Dr, Assistant Professor, School of Mechanical Engineering, Pusan National University, Busan, South Korea
-   *Yong-phil Jeon*, Dr., Precision Manufacturing System Division, Pusan National University, Busan, South Korea
-    *Marius Schwarz*, Dr., Assistant Professor, Department of Civil Engineering, University North, Varaždin, Croatia

**Copyright:** © Technobius, LLP

**Contacts:** Website: <https://technobius.kz/>  
E-mail: [technobiusphysics@gmail.com](mailto:technobiusphysics@gmail.com)

**CONTENTS**

<b>Title and Authors</b>	<b>Category</b>	<b>No.</b>
The creation a non-contact rotary mechanism powered by close-range ultrasonic energy <i>Dilnaz Khassenova, Albina Sarsenbayeva, Alibek Mussin</i>	<i>General Physics</i>	0004
Exploring the labyrinth of light: multiple Bragg Diffraction phenomena in face-centered cubic photonic crystals <i>Nurzhan Dosaev, Gulzhan Tulekova</i>	<i>Condensed Matter Physics</i>	0005
Experimental study of the influence of modified sulfur components on physical and mechanical characteristics of bitumen compositions <i>Tomiris Beisenbayeva, Anna Schmidt</i>	<i>General Physics</i>	0006



Article

## The creation a non-contact rotary mechanism powered by close-range ultrasonic energy

 Dilnaz Khassanova<sup>1,\*</sup>,  Albina Sarsenbayeva<sup>2</sup>,  Alibek Mussin<sup>2</sup>

<sup>1</sup>Department of General and Theoretical Physics, L.N. Gymilyov Eurasian National University, Astana, Kazakhstan

<sup>2</sup>Institute of Automation and Information Technologies, Almaty University of Power Engineering and Telecommunications, Almaty, Kazakhstan

\*Correspondence: [dilnaz.khassenova@mail.ru](mailto:dilnaz.khassenova@mail.ru)

**Abstract.** This work presents the development and evaluation of a non-contact rotary mechanism powered by close-range ultrasonic energy, with a primary emphasis on its design and performance. The pursuit of efficient, contactless rotary motion has gained significant importance in various industrial and technological applications. This study describes the innovative design of a rotary mechanism utilizing ultrasonic energy as the driving force, obviating the need for physical contact with rotating components. The design of this novel rotary mechanism leverages ultrasonic transducers to generate high-frequency vibrations, which are then transformed into rotational motion through a precisely engineered mechanism. The research explores the intricate details of the design, including the choice of materials, transducer placement, and resonance tuning to optimize performance. The mechanism's construction ensures low friction and minimal wear, making it a promising candidate for applications where reduced mechanical wear and maintenance are critical. Performance assessment of the ultrasonic rotary mechanism encompasses a comprehensive examination of key parameters, such as rotational speed, torque, power consumption, and efficiency. Experimental results reveal the mechanism's capability to achieve a high rotational speed while maintaining low energy consumption, thus underscoring its energy-efficient nature.  
**Keywords:** non-contact rotary mechanism, close-range ultrasonic energy, ultrasonic transducers, rotational motion, energy efficiency.

### 1. Introduction

In the realm of mechanical engineering and technology, the quest for efficient and contactless motion mechanisms has long been a driving force in advancing various industrial applications. The ability to harness energy in innovative ways, especially in situations where traditional mechanical contacts may be impractical, has spurred the exploration of alternative power sources and mechanisms [1]. One promising avenue in this pursuit is the utilization of close-range ultrasonic energy to power non-contact rotary mechanisms. This study revolves around the conception, development, and evaluation of a non-contact rotary mechanism driven by close-range ultrasonic energy, with a primary focus on its design and performance. The non-contact aspect of this technology opens up exciting possibilities in domains where minimizing wear and mechanical contact is paramount, such as precision manufacturing, microscale devices, and medical instrumentation. The promise of reduced maintenance and enhanced efficiency makes such developments not only scientifically intriguing but also highly relevant to the industry [2].

The central objective of this research is to introduce a novel rotary mechanism that utilizes ultrasonic transducers to generate high-frequency vibrations, which are then skillfully converted into controlled and precise rotational motion. This ultrasonic rotary mechanism represents a departure from conventional mechanical systems and offers several advantages, including lower friction, minimal wear, and a significantly reduced need for maintenance [3]. The design phase of this

mechanism is a key focus, encompassing critical considerations such as the selection of materials, transducer placement, and resonance tuning [4]. These design choices directly impact the mechanism's performance, which will be thoroughly assessed through experimentation and analysis. Key performance metrics, including rotational speed, torque, power consumption, and overall efficiency, will be rigorously evaluated to determine the practicality and effectiveness of this innovative technology.

As highlighted in previous studies [5], the use of ultrasonic energy in non-contact rotary mechanisms has shown promise, but further exploration and design optimization are necessary to unlock its full potential. Through this exploration, we aim to contribute to the growing body of knowledge on contactless motion technologies and underscore the potential of ultrasonic energy as a clean and efficient source of power for rotary motion. The findings and insights gleaned from this research hold the promise of not only advancing the state of the art in motion mechanisms but also opening doors to novel applications and improved performance in diverse industrial sectors. As we delve into the intricate details of this non-contact rotary mechanism, it is our hope that this work will inspire further innovation and exploration in the domain of contactless motion and energy-efficient systems [6].

Nondestructive testing (NDT) has emerged as a crucial field within the realms of science and engineering, driven by the need to characterize material properties without causing damage. Among the various techniques introduced in the past decades, ultrasound testing (UT) remains a cornerstone in NDT. Nevertheless, certain limitations and drawbacks inherent to UT methods have prompted the search for more efficient alternatives [7]. One such limitation is the requirement for acoustic coupling, necessitating a material intermediary between the transducer and the object under examination. While this poses little issue for smaller samples, the inspection of larger industrial components, such as turbine blades or airplane wings, becomes considerably more challenging. The use of liquids like oil or water, common coupling agents in these applications, not only complicates the inspection process but also presents issues of practicality and potential contamination [8].

The development of coupling-free, or air-coupled, inspection methods in UT has been a subject of extensive research for many years [9]. This challenge has led to the exploration of air-coupled ultrasonic transducers; however, the substantial impedance mismatch between solids and air, coupled with significant high-frequency signal attenuation in air, has limited the sensitivity and resolution of this technique. Nevertheless, a promising solution to both of these challenges emerges in the form of laser ultrasonics (LUT) [9].

Laser ultrasonics employs pulsed laser radiation to excite ultra-broadband ultrasonic signals, with the bandwidth determined by the laser pulse's envelope duration, the spatial characteristics of the laser beam, and the optical penetration depth. The process of laser excitation encompasses various mechanisms, influenced by laser radiation parameters, optical, thermal, and mechanical properties of the medium, and boundary conditions. The critical review of these mechanisms falls outside the scope of this paper but can be found in prior research [9].

Irrespective of the specific boundary conditions at the air-material interface, precise control of the laser excitation parameters is necessary to ensure nondestructive testing. Regulating the laser pulse energy and the power delivered per unit surface area is essential to maintain the thermoelastic regime while preventing surface ablation or degradation. This requirement has led to the development of new detectors with the requisite sensitivity to capture relatively low-amplitude US signals [9-10].

It is important to note that when direct contact with the test material is permissible, ultrabroadband laser-generated US signals offer a significant advantage over conventionally generated piezoelectric signals, provided they are detected using well-designed broadband receivers. Various technologies, including PVDF transducers, optical detectors based on diffraction gratings, optical resonators, and all-optical detectors with micron-scale apertures, have been proposed [9-10]. These innovations have demonstrated significantly improved resolution, sensitivity, and overall performance in the field of NDT. Recent breakthroughs in contact micron-scale aperture all-optical detectors have showcased unprecedented sensitivity, particularly for high-frequency applications

exceeding 20 MHz. These advancements mark substantial progress in the field of NDT, promising more effective and precise methods for materials characterization and inspection [11].

## 2. Methods

The research methodology for the creation and assessment of a non-contact rotary mechanism powered by close-range ultrasonic energy involves several key steps, including design, construction, and performance evaluation. This section outlines the methods employed in this study.

**Problem Definition:** Begin by defining the specific requirements and objectives of the non-contact rotary mechanism. Consider the desired rotational speed, torque, and energy efficiency.

**Material Selection:** Choose materials that are suitable for ultrasonic applications and the mechanism's intended use. Pay attention to the mechanical properties of these materials [12].

**Transducer Placement:** Determine the optimal placement of ultrasonic transducers to ensure efficient energy transmission to the rotary component. Consider factors such as resonance and vibration patterns.

**Mechanism Design:** develop a detailed design of the rotary mechanism, including its geometry, dimensions, and components. Utilize computer-aided design (CAD) software for precision.

**Resonance Tuning:** Perform resonance tuning to match the ultrasonic frequency to the mechanical resonance frequency of the mechanism for maximum energy transfer [13].

**Component Fabrication:** Fabricate the components of the rotary mechanism, including the transducers, rotary element, and support structure, using the selected materials and manufacturing techniques.

**Ultrasonic Transducers Integration:** Carefully integrate the ultrasonic transducers into the mechanism, ensuring secure attachment and alignment [14].

**Assemble the Mechanism:** assemble all components according to the design specifications, taking care to maintain precision and alignment.

**Experimental Setup:** Set up a controlled experimental environment with the necessary instrumentation, such as a tachometer, torque sensor, and power meter, to measure key performance parameters.

**Rotational Speed Measurement:** Conduct experiments to measure the rotary mechanism's rotational speed under different operating conditions, varying ultrasonic power levels, and load conditions [15-16].

**Torque Measurement:** Measure the torque generated by the ultrasonic rotary mechanism using a torque sensor to evaluate its mechanical performance.

**Power Consumption:** Record the power consumption of the ultrasonic transducers and the entire mechanism to determine its energy efficiency (Figure 1).

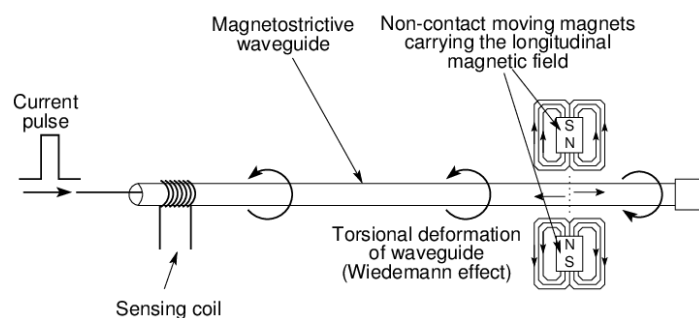


Figure 1 – Mechanism design of non-contact rotary mechanism

**Efficiency Analysis:** calculate the overall efficiency of the mechanism by comparing the input ultrasonic energy to the mechanical output, taking into account losses and friction.

**Wear and Maintenance Assessment:** Evaluate the mechanism for signs of wear or degradation over extended operation to assess the reduction in maintenance requirements.

Analyze the data collected from experiments to draw conclusions about the mechanism's performance, efficiency, and suitability for various applications. Compare the results to performance benchmarks or goals established during the design phase.

Validate the findings through repeated experiments and analysis to ensure the reliability and reproducibility of results. Iterate on the design and construction if necessary based on the results and insights gained during the evaluation phase.

Prepare a comprehensive report of the research

methodology, results, and conclusions, including visual aids such as graphs and charts to illustrate key findings. By following these methods, the research aims to create a robust non-contact rotary mechanism powered by close-range ultrasonic energy and rigorously evaluate its performance, energy efficiency, and potential for reduced maintenance in various applications.

### 3. Results and Discussion

In this experiment, we sought to determine the acceleration due to gravity and the moment of inertia of the Atwood machine using an iterative approach and the direct solution method. Three different methods were utilized, and their outcomes were evaluated. Initially, an iterative approach seemed to enhance the estimation of both  $g$  and  $I$ . Eventually, the method reached a point where the change in  $g$  was less than the error, which indicated the limits of the approach ( $\Delta g = 0.0293 \text{ m/s}^2$  and  $= 0.02731$ ). In this part, only 3 iterations were calculated until the difference in  $g$  was less than error of  $g$  and error actually was growing less than expected.

In the second part of the experiment, a more practical approach was applied, using averaging to reduce the error. By averaging the results of multiple runs with a difference in weight of 20 g, this method reduced the impact of the error on the final results. Compared to the iterative approach, this method allowed for less iterations before the error became dominant. However, it still faced limitations in terms of accuracy. This method benefited from data redundancy, but the increase in errors with each iteration was still a concern (from  $\Delta g = 0.0126 \text{ m/s}^2$  to  $\Delta g = 0.2849 \text{ m/s}^2$ ). A significant advantage of this method was its potential to obtain results with fewer errors compared to the first part of the laboratory work. Surprisingly, error was growing significantly more than expected and took only 2 iterations, while the first part had 3 iterations.

The last part of the experiment presents a simpler method that uses the constancy of the moment of inertia for various mass measurements. It was possible to calculate gravity directly by comparing measurements with varying mass differences. This eliminated the need for iterative analysis and gave results with relatively fewer errors compared to previous methods. However, results were not close to the true value of  $g$  ( $g_{avg} = 5.0751 \text{ m/s}$ ). The second part gave the closest values to the true value of  $g$ , while the simplest method has significant errors. More importantly, errors in part 3 were also more than in other parts.

### 4. Conclusions

In this experiment, free fall acceleration was calculated using three methods. First, an iterative method, where the overall result was  $7.8362 \text{ m/s}^2$ . Second, an iterative method including averaging, where  $g = 8.2531 \text{ m/s}^2$ . Third method gave the result - 5.0751 and 4.4201. Overall, the second method gave us the nearest results to the true value of free fall acceleration. Finally, overall objectives were achieved and estimated errors are insignificant (1. 0.0273, 2. 0.2849, 3. 0.3648). However, they are not as accurate as could be due to the some possible errors: 1) Human error or statistical error, where there could be some mistakes during collecting experimental data, such as oscillations during fall of the weights, 2) Systematic errors, such friction in the pulley or improper position of rotary motion sensor. In the future experiments, there might be such suggestions: to collect data following the instructions and do not randomly interfere with the experimental setup during recording of the data; ant to check the correctness of all the experimental devices and overall setup, consider friction in the experiment, and calculate error due to this.

### References

1. Air-coupled generation and detection of ultrasonic bulk waves in metals using micromachined capacitance transducers / D.W. Schindel // Ultrasonics. — 1997. — Vol. 35, No.2. — P. 179–181. [https://doi.org/10.1016/S0041-624X\(96\)00103-5](https://doi.org/10.1016/S0041-624X(96)00103-5)
2. Review of air-coupled ultrasonic materials characterization / D.E. Chimenti // Ultrasonics. — Vol. 54, No. 7. — P. 1804–1816. <https://doi.org/10.1016/j.ultras.2014.02.006>

3. Laser Optoacoustics / V. Gusev, A. Karabutov. — Maryland, USA: American Institute of Physics, 1993. — 130 p.
4. Laser Ultrasonics Techniques and Applications / C.B. Scruby, L.E. Drain. — Florida, USA: CRC Press, 1990. — 80 p.
5. Laser generation of acoustic waves in the ablative regime / T.W. Murray, J.W. Wagner // Journal of Applied Physics. — 1999. — Vol. 85, No. 4. — P. 2031–2040. <https://doi.org/10.1063/1.369498>
6. Novel combined optoacoustic and laser-ultrasound transducer array system / V. Simonova, E. Savateeva, A. Karabutov // Moscow University Physics Bulletin. — 2009. — Vol. 64, No. 4, P. 394–396. <https://doi.org/10.3103/S0027134909040092>.
7. The progress in photoacoustic and laser ultrasonic tomographic imaging for biomedicine and industry: A review / A. Bychkov, V. Simonova, V. Zarubin, E. Cherepetskaya, A. Karabutov // Applied Science. — 2018. — Vol. 8, No. 10. — P. 1931. <https://doi.org/10.3390/app8101931>
8. High-sensitivity compact ultrasonic detector based on a pi-phase-shifted fiber Bragg grating / A. Rosenthal, D. Razansky, V. Ntziachristos // Optics Letters. — 2011. — Vol. 36, No. 10. — P. 1833. <https://doi.org/10.1364/OL.36.001833>
9. Non-contact detection of ultrasound with light – Review of recent progress / J. Spytek, L. Ambrozinski, I. Pelivanov // Photoacoustics. — 2023. — Vol. 29. — P. 100440. <https://doi.org/10.1016/j.pacs.2022.100440>
10. A submicrometre silicon-on-insulator resonator for ultrasound detection / R. Shnaiderman, G. Wissmeyer, O. Ülgen, Q. Mustafa, A. Chmyrov, V. Ntziachristos // Nature. — 2020. — Vol. 585. — P. 372–378. <https://doi.org/10.1038/s41586-020-2685-y>
11. Looking at Sound: Optoacoustics with All-optical Ultrasound Detection / G. Wissmeyer, M.A. Pleitez, A. Rosenthal, V. Ntziachristos // Light: Science and Applications. — 2018. Vol. 17. — P. 1976. <https://doi.org/10.1038/s41377-018-00367>
12. Fabrication and characterization of High Q polymer micro-ring resonator and its application as a sensitive ultrasonic detector / T. Ling, S.-L. Chen, L.J. Guo // Optic Express. — 2011. — Vol. 19, No. 2. — P. 861–869. <https://doi.org/10.1364/OE.19.000861>
13. A transparent broadband ultrasonic detector based on an optical micro-ring resonator for photoacoustic microscopy / H. Li, B. Dong, Z. Zhang, H.F. Zhang, C. Sun // Scientific Reports. — 2015. — Vol. 4, No. 1. — P. 4496. <https://doi.org/10.1038/srep04496>
14. Comparative study of active infrared thermography, ultrasonic laser vibrometry and laser ultrasonics in application to the inspection of graphite/epoxy composite parts / V.P. Vavilov, A.A. Karabutov, A.O. Chulkov, D.A. Derusova, A.I. Moskovchenko, E.B. Cherepetskaya, E.A. Mironova // Quantitative InfraRed Thermography Journal. — 2020. — Vol. 17, No. 4. — P. 235–248. <https://doi.org/10.1080/17686733.2019.1646971>
15. Optical remote measurement of ultrasound / R.J. Dewhurst, Q. Shan // Measurement Science and Technology. — 1999. — Vol. 10, No. 11. — P. 139–168. <https://doi.org/10.1088/0957-0233/10/11/201>
16. Photoacoustic tomography and sensing in biomedicine / C. Li, L.V. Wang // Physics in Medicine & Biology. — 2009. — Vol. 54, No. 19. — P. 59–97. <https://doi.org/10.1088/0031-9155/54/19/R01>
17. Optical detection of ultrasound / J.P. Monchalin // IEEE Trans. Ultrasonic Ferroelectrics. — 1986. — Vol. 33, No. 5. — P. 485–499. <https://doi.org/10.1109/TUFFC.1986.26860>

### Information about authors:

*Dilnaz Khassenova* – Master Student, Department of General and Theoretical Physics, L.N. Gymilyov Eurasian National University, Astana, Kazakhstan, [dilnaz.khassenova@mail.ru](mailto:dilnaz.khassenova@mail.ru)

*Albina Sarsenbayeva* – MSc, Lecturer, Institute of Automation and Information Technologies, Almaty University of Power Engineering and Telecommunications, Almaty, Kazakhstan, [sarsenbayeva\\_1971@list.ru](mailto:sarsenbayeva_1971@list.ru)

*Alibek Mussin* – Master Student, Institute of Automation and Information Technologies, Almaty University of Power Engineering and Telecommunications, Almaty, Kazakhstan, [mussin07@mail.ru](mailto:mussin07@mail.ru)

### Author Contributions:

*Dilnaz Khassenova* – concept, methodology, funding acquisition, testing.

*Albina Sarsenbayeva* – interpretation, editing, modeling, resources.

*Alibek Mussin* – visualization, analysis, data collection, drafting.

*Received: 04.09.2023*

*Revised: 15.09.2023*

*Accepted: 18.09.2023*

*Published: 18.09.2023*



Article

## Exploring the labyrinth of light: multiple Bragg Diffraction phenomena in face-centered cubic photonic crystals

Nurzhan Dosaev, Gulzhan Tulekova\*

Physics Department, M. Kozbayev North Kazakhstan University, 13 Internatsionalnaya str., Petropavlovsk, Kazakhstan

\*Correspondence: [gulzhan.tulekova@bk.ru](mailto:gulzhan.tulekova@bk.ru)

**Abstract.** This work presents the outcomes of an experimental study aimed at exploring electron diffraction phenomena within a controlled environment. The experiment involved measuring the radii of diffraction rings produced under varying acceleration voltages, with a focus on the first-order ring. Unexpectedly, the observed values were half of the anticipated results, raising questions about the accuracy of the measurements. The analysis revealed that the measured value of  $d_1$  closely resembled the theoretical value of  $d_2$ , suggesting a potential oversight of the first diffraction ring, possibly due to its diminutive size. The high brightness of the incident light further complicated the measurement process. Accounting for the possibility of overlooking the first diffraction ring, the derived values for  $d_2$  ( $128.24 \pm 33.26$  pm) and  $d_3$  ( $70.00 \pm 5.21$  pm) were compared to theoretical values (123 pm and 80 pm, respectively). Despite the challenges, the experimental results fell within an acceptable range, considering the inherent uncertainties. To mitigate errors in radii measurement, the article suggests the implementation of an automated system and recommends a thorough reassessment of experimental setup configurations to optimize conditions for more accurate measurements. The findings highlight the importance of methodological refinement to enhance precision and reliability in electron diffraction studies. This work contributes valuable insights to the field and underscores the continuous need for advancements in experimental techniques.

**Keywords:** photonic crystals, crystallography, face-centered cubic, diffraction phenomena, labyrinth of light.

### 1. Introduction

Bragg's law elucidates the relationship between the wavelength of incident radiation and the angle at which it is scattered by lattice planes, resulting from the constructive interference of wave fronts [1]. The phenomenon of Bragg diffraction contributes to the emergence of band gaps within the energy spectra of diverse periodic structures. Among these structures are photonic crystals (PhCs) [1–4], characterized by band gaps within the electromagnetic spectrum. The position of these gap energies is determined by the periodic modulation of the dielectric constant [1–4].

In the context of light Bragg diffraction, understanding the processes occurring at the surface of the Brillouin zone (BZ) where photonic stop bands emerge is crucial. Bragg diffraction manifests when the Laue conditions are met:  $k_s = k_i + g_{hkl}$ , where  $k_s$  and  $k_i$  represent the wave vectors of the incident and scattered light waves, respectively,  $g_{hkl}$  indeed determined by a system of scattering planes with Miller indices (hkl) [1–4].

Scientists have established that the quality of graphite is primarily characterized by its carbon content and structural properties [5]. Unlike a single crystal, graphite does not exist as a single mineral formation; it predominantly exists in the form of aggregates consisting of graphite and its enrichment products. In addition, various structure less carbon phases may be present along with graphite. The properties of these materials are influenced not only by the carbon content, but also by the amount and arrangement of crystalline, or ordered, graphite - in essence, the texture and structure of the material. Therefore, to accurately assess the properties of graphite samples, it is necessary to consider both their crystal structure and the texture and structure of all components present [5–9].

The research team published a paper [10] that displayed the effects observed when soft carbon materials undergo annealing at high temperatures or when graphite is subjected to disordered-inducing processes such as fast neutron irradiation or mechanical grinding.

X-ray structural analysis is commonly employed to explore the crystalline arrangement of carbon materials like graphite [11]. This method allows for the assessment of the structure's level of organization and the dimensions of its crystallites, which are the smallest building blocks of the structure. The composite data collected from diverse sources indicates characteristic interlayer spacings at approximately 3.38 Å, 3.40 Å, 3.425 Å, 3.44 Å, and 3.55 Å, along with one notably observed around 3.68 Å [11–14].

In this paper, the lattice properties of graphite were studied in detail using X-ray irradiation. The X-ray irradiation method provided information about the structure of graphite and its characteristics.

## 2. Methods

The experiment investigates the wave-particle duality of electrons through the diffraction of fast electrons by a polycrystalline graphite layer, a phenomenon analogous to the diffraction of light. As the electrons interact with the graphite crystal lattice, they exhibit wave-like behavior, generating interference patterns in the form of concentric rings on a fluorescent screen [11–13]. The primary objective of the experiment is to measure the diameter of these diffraction rings at various accelerating voltages to determine the interplanar spacing within the graphite structure. By applying the principles of electron diffraction and Bragg's law, the interplanar spacings are calculated using the observed ring diameters and the known accelerating voltages [13–14]. This experiment thus serves to elucidate the fundamental properties of crystal structures and to reinforce the dual nature of electrons as both particles and waves.

The electron diffraction apparatus is a comprehensive assembly designed to probe the wave-particle duality of electrons via their interaction with a crystalline structure. Central to this setup is the Electron Diffraction Tube, meticulously mounted to ensure the precise trajectory of electrons towards the target polycrystalline graphite layer. This tube is the heart of the experiment, where the crucial phenomenon of electron diffraction occurs.

To facilitate the acceleration of electrons to the requisite high speeds, a High Voltage Supply Unit is employed, capable of delivering an adjustable voltage ranging from 0 to 10 kV. The flow of electrons is carefully regulated by a 10 MOhm High-value Resistor, which serves to limit the current and provide an additional layer of safety against electrical surges.

The intricate connections within the apparatus are made possible by specialized Connecting Cords rated for 50 kV, with a standard length of 500 mm, ensuring safe transmission of high voltage to the diffraction tube. Additionally, a separate Power Supply unit, adjustable up to 600 V, is utilized for precise control over the electron beam and to power ancillary components of the setup.

Measurements of the resulting diffraction patterns are taken with a Vernier Caliper made of plastic, chosen for its non-conductive properties, which is essential for maintaining safety in an environment where high voltages are present. The caliper's precision allows for accurate determination of the ring diameters, which are pivotal for calculating the interplanar spacings in the graphite lattice.

The apparatus also includes an assortment of Connecting Cords in various lengths—250 mm and 750 mm—and colors—red, blue, yellow, and black. These cords not only facilitate a secure and organized connection between the various components but also adhere to standard color coding practices to aid in the correct setup. Red and blue cords typically denote positive and negative connections, respectively, while yellow and black cords are used for grounding or common connections.

Together, these components form a sophisticated system that, when correctly assembled and calibrated, enables the detailed study of electron diffraction patterns. The careful design and selection

of each element ensure that the apparatus functions safely and effectively, providing valuable insights into the quantum nature of electron behavior and the structural properties of crystalline materials.

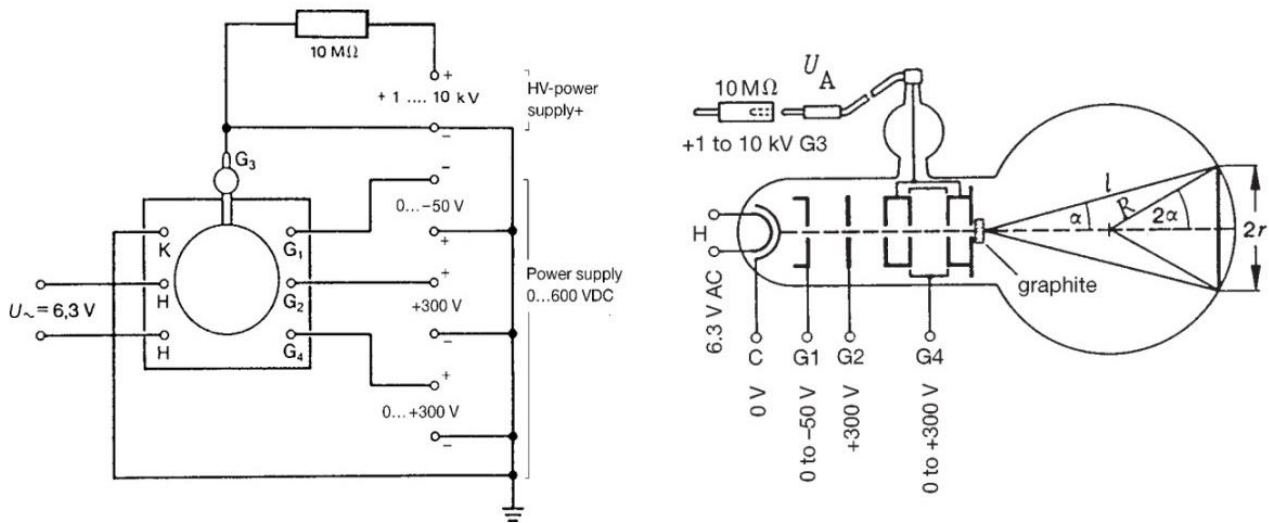


Figure 1 – Schematic diagram of the o the electron diffraction tube

The experimental apparatus was arranged in accordance with the schematic representation depicted in Figure 1. The electron diffraction tube was integrated into the experimental setup, with its sockets meticulously connected to the power supply following the configuration illustrated in Fig. 2. Notably, a secure connection was established between the high voltage and the anode G3 through a  $10\text{ M}\Omega$  protective resistor.

To ensure optimal diffraction outcomes, precise adjustments were made to the Wehnelt voltage G1, as well as the voltages G4 and G3. These adjustments were meticulously calibrated to elicit the formation of sharp and well-defined diffraction rings. The resultant diffraction pattern was subjected to analysis for further insights into the underlying electron behavior.

An essential step in the experimentation process involved reading the anode voltage directly from the display of the high-voltage power supply. This voltage measurement served as a critical parameter for subsequent analyses and interpretations.

In order to ascertain the dimensions of the diffraction rings, careful measurements were conducted using a Vernier caliper. In a controlled, darkened room environment, both the inner and outer edges of the diffraction rings were meticulously measured, and the obtained values were used to compute an average diameter. It is important to note the presence of an additional faint ring, situated immediately behind the second ring, highlighting the complexity of the diffraction pattern and the need for comprehensive analysis. This experimental approach adheres to established protocols in electron diffraction studies, ensuring precision and reliability in the acquisition of data and subsequent interpretations.

### 3. Results and Discussion

The interference phenomenon observed in electron diffraction experiments can be explained through the concept of wave-particle duality, which is a cornerstone of quantum mechanics [15–16]. According to this concept, particles such as electrons exhibit both particle-like and wave-like properties. When electrons pass through a crystalline structure, they interfere with each other in a manner similar to waves, creating a pattern of constructive and destructive interference that can be observed and measured.

By substituting the momentum into the de Broglie equation [17–18], the wavelength of the electrons can be calculated. This wavelength is crucial for understanding the interference patterns observed in the experiment, as it allows for the application of Bragg's law to determine the interplanar

spacing of the crystalline structure being used. In the described experiment, a diffraction tube along with the requisite equipment was utilized to explore the wave-like characteristics of particles, specifically electrons. The experiment hinged on the principle of electron diffraction, where electrons demonstrate wave behavior when passed through a crystalline structure, such as graphite.

The electron diffraction experiment was conducted within a glass bulb with a specified radius of 65 mm. The diffraction patterns for the first-order ring were observed and measured across varying voltages, yielding data as presented in Tables 1 and 2. Table 1 provides diameter measurements for the first-order ring at voltages ranging from 4.0 kV to 6.5 kV.

Table 1 – Voltage levels ranging from 4.0 kV to 6.5 kV and corresponding measurements of the first-order ring's diameter

Voltage V, <i>kV</i>	Inner Diameter, $\pm 0.05$ mm	Outer Diameter, $\pm 0.05$ mm
4.0	28.78	36.51
	50.15	61.11
4.5	21.03	30.98
	46.74	55.48
5.0	24.68	30.28
	42.75	50.12
5.5	22.31	27.73
	41.02	46.13
6.0	21.34	24.97
	38.12	43.88
6.5	21.01	24.75
	35.14	42.02

It is imperative to note that the diameter measurements were obtained using a Vernier caliper in a controlled environment. The precision of the measurements, coupled with the systematic variation of voltage, provides a comprehensive dataset for the analysis of electron diffraction behavior within the specified experimental setup.

Table 2 – Voltage levels ranging from 7.0 kV to 9.9 kV and corresponding measurements of the first-order ring's diameter

Voltage V, <i>kV</i>	Inner Diameter, $\pm 0.05$ mm	Outer Diameter, $\pm 0.05$ mm
7.0	19.47	25.02
	34.05	39.15
7.5	19.04	20.14
	32.38	36.75
8.0	17.15	19.46
	31.13	35.38
8.5	17.41	19.06
	31.14	34.98
9.0	17.11	20.05
	28.72	33.45
9.5	16.63	17.65
	26.98	32.15
9.9	16.75	18.15
	27.03	30.03

Each entry includes both inner and outer diameter values, with a precision of  $\pm 0.05$  mm. Notable variations in diameter are observed with changes in voltage, indicating the sensitivity of the diffraction pattern to applied electrical potentials. Similarly, Table 2 details diameter measurements

for the first-order ring at higher voltages, ranging from 7.0 kV to 9.9 kV. The precision of  $\pm 0.05$  mm is maintained for both inner and outer diameter values. Again, the data underscores the impact of increased voltage on the dimensions of the diffraction ring.

Table 3 – The wavelength of the electrons under a certain acceleration voltage

Voltage $U_A, kV$	Wavelength, $pm$	The error of wavelength, $pm$
4.0	19.19	0.127
4.5	18.18	0.130
5.0	17.34	0.114
5.5	16.53	0.113
6.0	15.76	0.110
6.5	15.14	0.106
7.0	15.03	0.103
7.5	15.16	0.098
8.0	13.72	0.097
8.5	13.28	0.096
9.0	13.03	0.085
9.5	12.51	0.081
9.9	12.34	0.077

The dataset reveals a consistent trend wherein as the acceleration voltage increases, the electron wavelength decreases. This relationship is pivotal for understanding the behavior of electrons under varying electrical potentials. The associated error values underscore the meticulous nature of the measurements, ensuring the accuracy of the reported electron wavelengths.

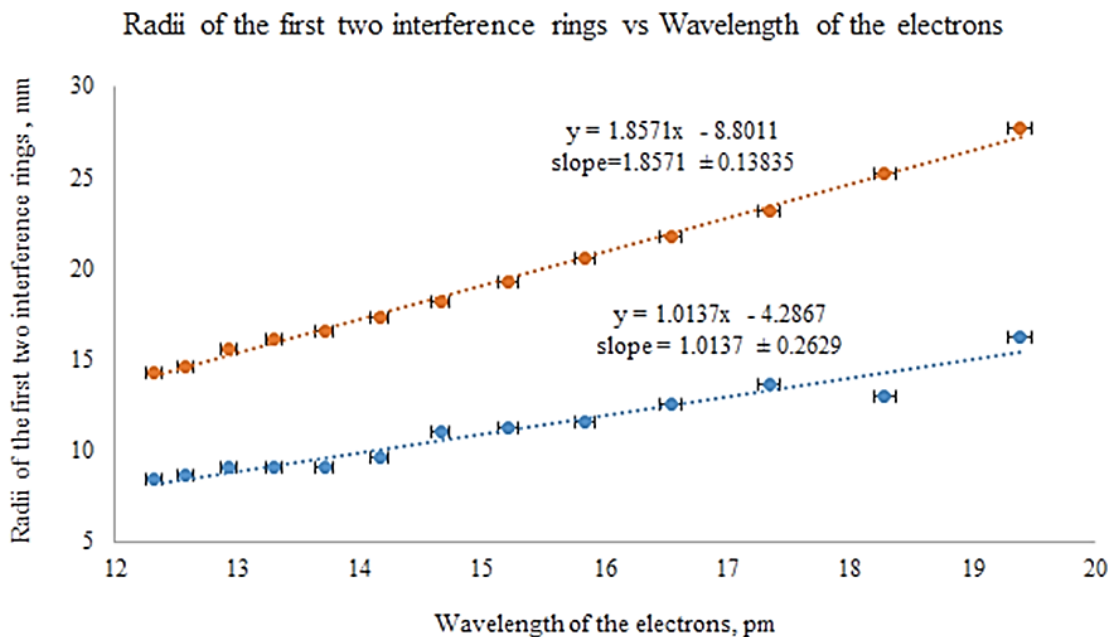


Figure 2 – Diameters of the initial two diffraction rings compared to the electron wavelength

These findings contribute to the broader comprehension of electron dynamics and wave-particle duality within the experimental framework.

The wavelength data, coupled with the associated errors, serves as a valuable resource for further analysis, theoretical modeling, and the advancement of knowledge in the field of electron diffraction studies.

As it can be seen, we observed some sort of unexpected results. We got values half as much as expected. Furthermore, according to the results of this experiment, the value of  $d_1$  is closer to the

theoretical value of  $d_2$  and the value of  $d_2$  is closer to the theoretical value of  $d_3$ . We obtained results as if we were measuring the radii of second and third visible diffraction rings. It might be possible if the first ring was much smaller than the second and the third rings.

The brightness of incident light could have potentially worsened the situation so that we could not clearly see the first diffraction ring.

If we treat the experimental value of  $d_1$  as the theoretical value of  $d_2$  and the experimental value of  $d_2$  as the theoretical value of  $d_3$ , we can conclude that the experiment was conducted successfully. However, the error of  $d_1$  is comparable with the calculated value.

This is because data points for  $d_1$  are not within the desired margin so that they would have a good linear fit with a small slope error. It possibly might have been the result of systematic error in measuring diffraction rings' radii because those diffraction rings have very blurry boundaries and precisely measuring the inner and outer radii of the first diffraction ring is difficult for small values. This explains why  $d_1$  has a greater error than  $d_2$ .

We can mitigate the issue with radii measuring if we will use a sort of automatic measuring system that would easily measure inner and outer radii without cognitive biases that humans have. Also changing configurations so that diffraction rings are easier to measure can improve the situation with the error of  $d_1$ .

#### 4. Conclusions

In a broader context, the success of the experiment hinges on the assumption that the measured parameters correspond to interplanar spacings  $d_2$  and  $d_3$ , while the diffraction ring associated with  $d_1$  may have been sufficiently small to escape detection. The heightened brightness of the incident light potentially exacerbated this situation. Considering the possibility of overlooking the first diffraction ring, the derived values suggest that  $d_2$  is  $128.24 \pm 33.26$  pm and  $d_3$  is  $70.00 \pm 5.21$  pm. In comparison, the theoretical values for  $d_2$  and  $d_3$  are 123 pm and 80 pm, respectively. Remarkably, the experiment's results fall within an acceptable range, considering the inherent uncertainties.

To address the error in measuring diffraction ring radii, implementing an automated system is recommended, offering a potential solution by minimizing human-induced biases. Additionally, a careful reassessment and optimization of the experimental setup configurations are essential. Identifying ideal conditions under which diffraction rings are more easily measurable can significantly enhance the precision and reliability of the experimental outcomes. These considerations underscore the continuous need for refinement in methodology to ensure the accuracy of results and contribute to the advancement of scientific knowledge in the field.

#### References

1. Multiple Bragg diffraction in opal-based photonic crystals: Spectral and spatial dispersion / I.I. Shishkin, M.V. Rybin, K.B. Samusev, V.G. Golubev, M.F. Limonov // *Physical Review B*. — 2014. — Vol. 89. — P. 035124. <https://doi.org/10.1103/PhysRevB.89.035124>
2. *Photonic Crystals: Molding the Flow of Light* / J.D. Joannopoulos, S.G. Johnson, J.N. Winn, R.D. Meade. — Princeton, USA: Princeton University Press, 2018. — 305 p.
3. *Optical Properties of Photonic Crystals* / K. Sakoda. — New York, USA: Springer, 2004. — 258 p.
4. *Optical Properties of Photonic Structures: Interplay of Order and Disorder* / M.F. Limonov, R.M. De La Rue. — Florida, USA: CRC Press, Taylor & Francis Group, 2012. — 528 p.
5. *Crystallographic Analysis of Graphite by X-Ray Diffraction* / A.N. Popova // *Chemistry*. — 2017. — Vol. 60. No. 9. — P. 361-365. <https://doi.org/10.3103/S1068364X17090058>
6. *Interstitials in graphite and disordered carbons* / J. Lachter, R.H. Bragg // *Physical Review B*. — 1986. — Vol. 33. No. 12. — P. 8903. <https://doi.org/10.1103/PhysRevB.33.8903>
7. *XRD Characterization of the Structure of Graphites and Carbon Materials Obtained by the Low-Temperature Graphitization of Coal Tar Pitch* / Ch.N. Barnakov, G.P. Khokhlova, A.N. Popova, S.A. Sozinov, Z.R. Ismagilov // *Eurasian Chemico-Technological Journal*. — 2015. — Vol. 17. — P. 87–93.
8. *Chemistry and Physics of Carbon: Volume 7* / D.B. Fischbach (edited by P. L. Walker, Jr.). — New York, USA: Marcel Dekker, 1971. — 403 p.

9. In Proceeding of the Second Conference on Industrial Carbon and Graphite / B. Pandic. — Society of Chemical Industry, New York, USA: Gordon and Breach, 1966. — 654 p.
10. Anisotropy factors of polycrystalline graphites / W.N. Reynolds // *Carbon*. — 1968. — Vol. 6. No. 3. — P. 277-282. [https://doi.org/10.1016/0008-6223\(68\)90023-7](https://doi.org/10.1016/0008-6223(68)90023-7)
11. Structural disorder induced in graphite by grinding / M. Tidjani, J. Lachter, T.S. Kabre, R.H. Bragg // *Carbon*. — 1968. — Vol. 24. No. 4. — P. 447 – 449. [https://doi.org/10.1016/0008-6223\(86\)90266-6](https://doi.org/10.1016/0008-6223(86)90266-6)
12. The diffraction of short electromagnetic waves by a crystal / W.L. Bragg // Cambridge Philosophical. Society. — 1913. — Vol. 17. — P. 43–57.
13. Photonic Crystals: Molding the Flow of Light / J.D. Joannopoulos, S.G. Johnson, J.N. Winn, R.D. Meade. — Princeton, USA: Princeton University Press, 2008. — 305 p.
14. Inhibited spontaneous emission of quantum dots observed in a 3D photonic band gap / M.D. Leistikow, A.P. Mosk, E. Yeganegi, S.R. Huisman, A. Lagendijk, W.L. Vos // *Physical Review Letters*. — 2011. — Vol. 107, No. 19. — P. 193903. <https://doi.org/10.1103/PhysRevLett.107.193903>
15. Observation of sub-Bragg diffraction of waves in crystals / S.R. Huisman, R.V. Nair, A. Hartsuiker, L.A. Woldering, A.P. Mosk, W.L. Vos // *Physical Review Letters*. — 2012. — Vol. 108, No. 8. — P. 083901. <https://doi.org/10.1103/PhysRevLett.108.083901>
16. Diffraction of light from thin-film polymethyl methacrylate opaline photonic crystals / S. G. Romanov et al // *Physical Review Letters*. — 2001. — Vol. 63, No. 5. — P. 056603. <https://doi.org/10.1103/PhysRevE.63.056603>
17. Polarized light coupling to thin silica-air opal films grown by vertical deposition / A. V. Baryshev et al. // *Physical Review Letters*. — 2007. — Vol. 76, No. 1. — P. 014305. <https://doi.org/10.1103/PhysRevB.76.014305>

### **Information about authors:**

*Nurzhan Dosaev* – Master Student, Physics Department, M. Kozbayev North Kazakhstan University, 13 Internatsionalnaya str., Petropavlovsk, Kazakhstan, [dosayev.n@gamil.com](mailto:dosayev.n@gamil.com)

*Gulzhan Tulekova* – Master Student, Physics Department, M. Kozbayev North Kazakhstan University, 13 Internatsionalnaya str., Petropavlovsk, Kazakhstan, [gulzhan.tulekova@bk.ru](mailto:gulzhan.tulekova@bk.ru)

### **Author Contributions:**

*Nurzhan Dosaev* – concept, methodology, data collection, analysis, visualization, drafting.

*Gulzhan Tulekova* – resources, testing, modeling, interpretation, editing, funding acquisition.

*Received: 8 September 2023*

*Revised: 25 September 2023*

*Accepted: 28 September 2023*

*Published: 28 September 2023*



Article

## Experimental study of the influence of modified sulfur components on physical and mechanical characteristics of bitumen compositions

 Tomiris Beisenbayeva<sup>1,\*</sup>,  Anna Schmidt<sup>2</sup>

<sup>1</sup>School of Engineering and Digital Sciences, Nazarbayev University, 53 Kabanbay ave., Astana, Kazakhstan

<sup>2</sup>Faculty of Mechanical engineering, University of Applied Sciences Duesseldorf, 156 Münsterstraße st., Duesseldorf, Germany

\*Correspondence: [tbeisenbayeva@mail.ru](mailto:tbeisenbayeva@mail.ru)

**Abstract.** In this research work, the physical, mechanical and performance characteristics of bituminous binder 90/130 before and after its modification with sulfur in the proportions of 10%, 30% and 50% of the binder weight were analyzed. Experimental results showed the effect of sulfur content on the mechanical characteristics of bituminous binder. By elemental analysis of the spectra of modified bitumen binder samples, it was found that there were no significant chemical changes with increasing sulfur content. The formation of new chemical compounds was not revealed, which is confirmed by the absence of new characteristic peaks in the spectra. Analysis and comparison of the experimental data of softening temperature showed an insignificant influence of the liquid heating rate on the concentration of the modifying agent. However, the increase of sulfur concentration more than 10% in the modified bitumen leads to an increase in softening temperature. This is due to the formation of denser structure and increase in viscosity of bitumen with increasing amount of sulfur in the system. Thus, the presence of sulfur as a dispersed phase in polymer bitumen has a natural effect on the mechanical characteristics of sulfur asphalt concretes, leading to an increase in their mechanical properties with increasing sulfur content.

**Keywords:** bituminous binders, modified bitumen, sulfur, ring and ball method, softening point, penetration.

### 1. Introduction

Modern highways, especially those subjected to significant dynamic loads, as well as airfield runways and cargo areas, require high quality standards for their asphalt concrete pavements [1]. Petroleum bitumens, which are dispersed colloidal systems of complex chemical composition, are used as road binders. To improve the quality and durability of road surfaces, modified road binders are now widely used [2]. The modification process is aimed at improving the properties of bitumen by combining it with special components.

Nowadays, not pure bitumen, but modified with different components, the main difference of which is higher performance characteristics and qualities, is used quite actively in the field of construction [3-6].

Studies on the use of sulfur as a modifying constituent in bituminous binders have started relatively recently and are not fully understood [7]. Crystalline sulfur, produced as are product in the oil and gas industry, it's an available resource that, when in solid state, is non-toxic and has high chemical resistance in a variety of aggressive industrial environments [8].

The authors of the works revealed [9, 10] that sulfur not only serves as a mixture filler, but also acts as a stabilizer of bitumen mixture. Another work presents that the addition of sulfur content in paving materials above 30%, with the correct design and methodology of bitumen binder modification, leads to effective stabilization of these materials [9].

According to standard normative documents [11], one of the key indicators of binders are the values of softening point and brittleness temperature. The working range of a binder is defined as the difference between the brittleness temperature (usually below  $-17^{\circ}\text{C}$ ) and the softening point (usually above  $+43^{\circ}\text{C}$ ). In this range, the substance is in a visco-plastic state characterized by moderate plasticity without brittleness and the ability to retain shape without fluidity under small shear loads. Thus, materials based on such a binder have the required consumer properties, such as moderate ductility and shear stability, over the operating temperature range.

Due to the need to ensure the stability of bituminous binder properties at all stages of the technological process there is a need to improve a set of methods for assessing its quality.

This paper presents the results of research into one of the most effective directions in road construction - modification of petroleum road bitumen and obtaining sulfur asphalt concrete on their basis.

## 2. Methods

In this study, a consecutive series of experiments was carried out in order to identify in detail the nature of interaction between gray and oil bitumen. The object of the study was oil road bitumen 90/130 produced by Promstroybitum, LLP, corresponding to [11].

In the manufacture of sulfur-bitumen binder was used granulated crystalline sulfur according to [12] in proportions of 10%, 30% and 50% of bitumen weight. The process of modification was carried out by heating on a water bath to  $100^{\circ}\text{C}$  of pure bitumen grade 90/130 and adding sulfur and with careful and continuous stirring with a propeller mixer at a speed of 100 rpm for 90 min. Multi-element analysis of a wide range of matrices of modified bitumen was carried out on a Rigaku EDXRF spectrometer (Japan), which use X-rays in the energy range 1-65 eV and photoelectric effect to determine the elemental composition.

The study of mechanical properties of modified bitumen was based on the study of mechanical properties of the base sample of bitumen 90/130 relative to the samples with the addition of sulfur.

To determine the thermal sensitivity and resistance of the sample of bitumen 90/130 to deformation, studies of its softening temperature ( $T_s$ ) were carried out on the automatic equipment B072 "Automatic apparatus ring and ball" of the company "Matest" (Italy). Two chromium-plated rings of step form were filled with 6 g of base bitumen without modifier each. For the purpose of additional fixation two centering rings and two steel balls  $\varnothing 9.5$  mm. each were placed on top of them. The finished samples were mounted in a special brass frame for immersion in a beaker made of pyrexerglass, i.e. the medium. Freshly distilled cooled distilled water of 600 ml volume was used as a thermoregulating medium. The process of water heating not exceeding  $80^{\circ}\text{C}$  was carried out using an integrated glass-ceramic heating surface providing a heating rate of  $5^{\circ}\text{C}/\text{min}$ . in accordance with the requirements of [11]. Uniform heating was provided by the built-in magnetic stirrer with electronic speed controller, capable of providing rotation in the range from 0 to 160 rpm. The temperature sensor connected to the B072 apparatus was inserted in the center of the brass frame, providing accurate recording of the temperature change of the medium. Two integrated laser sensors were used to record the ball drop moment used to determine the softening temperature. These were placed on either side of a beaker containing distilled water. The difference in  $T_s$  between the base and modified bitumen is not more than  $1^{\circ}\text{C}$ , which is within the normalized measurement error.

Studies of specific viscosity of modified bitumen were carried out on penetrometer B056-02 KIT of "Matest" (Italy). Penetration was subjected to modified bitumen with a mass of 1500 g., preheated in a steam bath to  $100^{\circ}\text{C}$ . Penetrometer equipped with digital micrometric adjustment was automatically fixed at zero position at the boundary of the needle and modified bitumen touching. Special 50 g and 100 g weights were mounted on the penetrometer to ensure vertical penetration of the standard needle. A magnetic controller with an electronic digital programmable timer, automatically releasing the plunger head with the specified mass, ensured free fall of the needle during the 5-second test. Depth, penetration time and sample temperature were recorded automatically.

### 3. Results and Discussion

In order to control the process of bituminous binder modification and to determine the chemical composition of bitumen 90/130 after modification with sulfur in the proportions of 10%, 30% and 50% of the initial sample weight, elemental analysis was carried out on a Rigaku EDXRF spectrometer in the energy range from 4 to 23 eV (Figure 1).

Graph 1 shows the spectra of elemental analysis of bitumen 90/130 before and after modification with sulfur 10%, 30% and 50%. In the obtained spectra intense characteristic peaks of bitumen 90/130 binder at 17 eV and 18 eV corresponding to stretching vibrations of C-H noodles in  $\text{CH}_2$  elements are noticeable. These peaks indicate the presence of a high concentration of arene in bitumen binder [13].

The first observed peak around 4.5 eV corresponds to deformation vibrations of  $\text{CH}_2$  elements in alkane pairs. Three consecutive peaks with energies of 4.6 eV, 5.0 eV and 5.2 eV indicate out-of-plane vibrations of CH and also indicate the presence of arene compounds. These results are in agreement with previous studies [13], confirming the structural features and composition of the bituminous binder.

Further analysis of the spectra demonstrates an insignificant change in intensity at energies of 6.3 eV, 6.6 eV and 9.7 eV. The absence of significant peaks in these regions indicates that the modification of bituminous binder 90/130 does not lead to significant changes in its chemical composition. In other words, new chemical compounds formed due to the interaction of sulfur and oil bitumen were not detected. Similar results were obtained earlier in other studies [14], which confirms the continuity of this phenomenon. The intense peaks found around 8.5 eV and 9 eV correspond to the strain vibrations  $\delta(\text{CH}_3)$  and  $\delta(\text{CH}_2)$ , respectively. These maxima are characteristic of saturated hydrocarbons, paraffins, and oils.

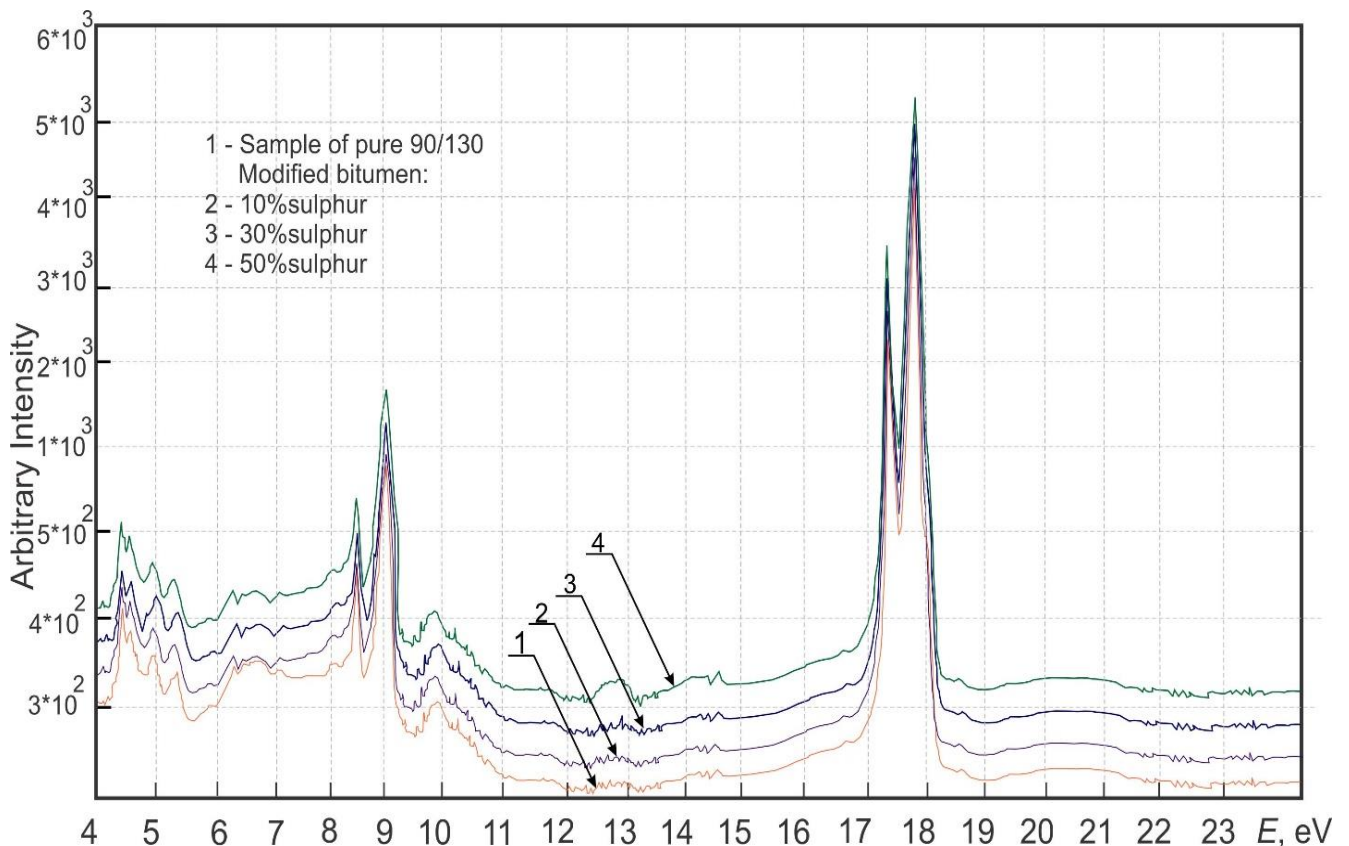


Figure 1 – Elemental analysis of a wide range of modified bitumen: 1 – Pure 90/130; 2 – modified bitumen with 10% sulphur; 3 – modified bitumen with 30% sulphur; 4 – modified bitumen with 50% sulphur

The maximum at 9.9 eV corresponds to stretching vibrations of C=C noodles; this feature is observed both in the spectra of the original sample bitumen 90/130 and in the spectra of sulfur-modified bitumen. The structural complexity of this band indicates the extensive presence of arene elements in the bitumen composition, including asphaltenes and other components [15].

When analyzing the spectra, it was also found that both the sample of the original bitumen 90/130 and the sample of modified bitumen with the addition of 10% sulfur contain bound water. This is confirmed by the presence of bands with peaks at 19 eV and 20 eV, which shows to stretching vibrations of the oxygen-hydrogen bond in hydroxyl groups involved in the formation of intermolecular hydrogen bonds. However, for samples with 30% and 50% sulfur content, these peaks are less intense, indicating less water. This suggests a potential improvement in performance properties, such as frost resistance, for bituminous binders with 30% and 50% sulfur content.

The results of the study of physical and mechanical properties of the modified binder indicate the effect of changing the concentration of sulfur on all analyzed characteristics of the binder. At the same time, the analysis of concentration dependences confirms the linear relationship between the sulfur concentration and the relative change in these properties.

Figure 2 shows the temperature dependence of the heating rate of the medium, demonstrating that increasing sulfur concentration leads to an increase in the  $T_s$  at all heating rates. The  $T_s$  is indicated as the average value of temperatures at a fixed rate at which two disks soften sufficiently for each ball wrapped with binder to fall a distance of 25 mm. The analysis of the results shows that varying the heating rate within 0.5 °C causes an error in the  $T_s$  measurement between 1.0 and 1.5 °C.

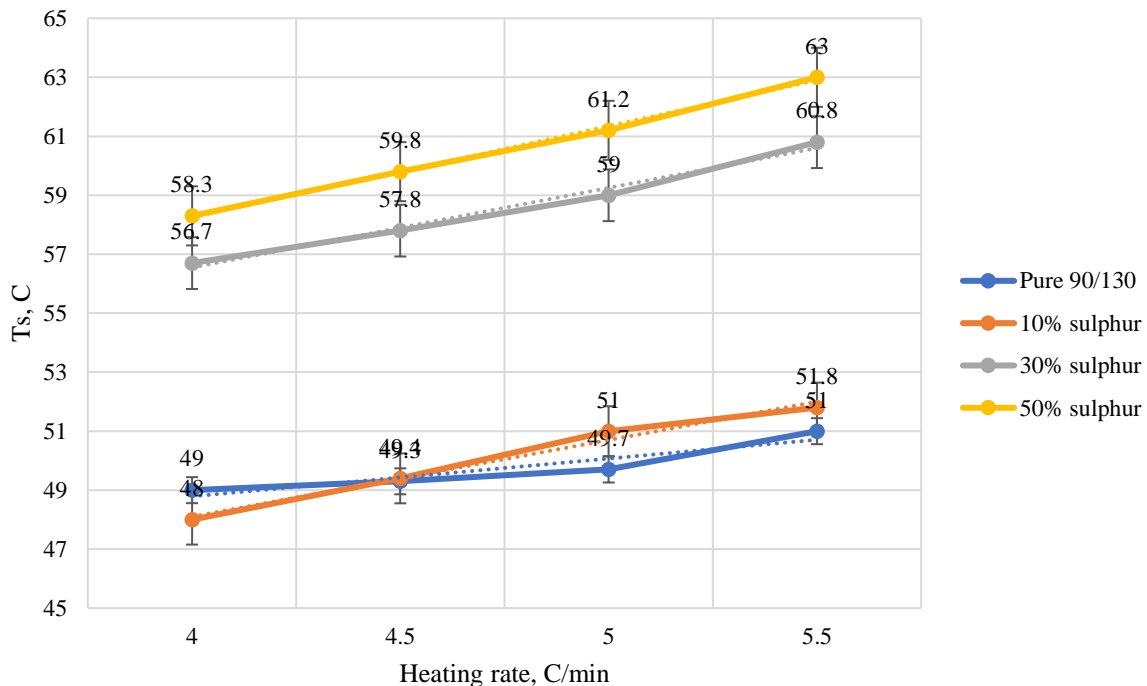


Figure 2 – Effect of medium heating rate on softening point of bitumen 90/130 before and after modification

From the graph 2 shows that the initial sample of bituminous binders grade 90/130 did not show a significant effect on the range of operating temperatures. However, at a concentration of sulfur not exceeding 10%, there is a decrease in softening temperature by 10%. This effect can be explained by the insufficient amount of sulfur formed and its low molecular weight, which does not contribute to the formation of a spatial mesh of the polymer, improving the working temperature range. When increasing the concentration of sulfur as a filler, the amount of formed mixture increases significantly, which leads to a marked increase in the viscosity of the system and, consequently, an increase in the softening temperature. It is worth noting that when introducing crystalline sulfur into bitumen 90/130

in the amount of 10%, 30% and 50% of the mass of the binder, the physical and chemical parameters meet the requirements of RK 218-145-2019.

One of the important parameters of physical and mechanical properties of binders is the measure of resistance under gravity. Studies on the effect of temperature on the penetration depth at 25°C of binders can be considered optimal, because such data allow us to evaluate the behavior of the material under conditions of comfortable temperature, which can be significant in the design and use of materials in different climatic zones [16].

To evaluate the dynamic viscosity of modified bitumen, we conducted studies aimed at revealing the dependence of penetration depth on temperature when adding weights weighing 50 g and 100 g, the data of which are shown in Figures 2 - 3.

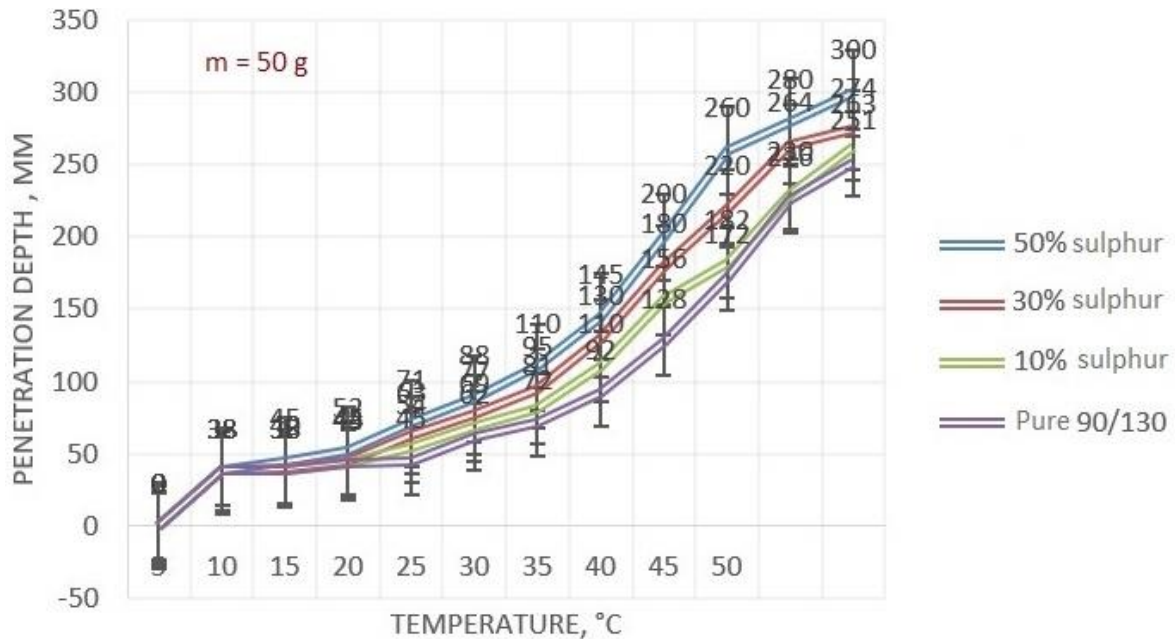


Figure 3 – Dependence of penetration depth on temperature of bitumen 90/130 before and after modification with additional mass of 50 g

Figure 3 shows the results of the analysis, which indicate that the changes in the properties of sulfur-bitumen binder associated with an increase in sulfur content. Note that to a large extent such changes are due to the presence of an additional dispersed phase due to physically free sulfur, which significantly affects the viscosity of the materials. Diagram 3 shows that at a standard temperature of 25°C and a mass of 50 g. the depth of penetration of the needle in the original sample of bitumen grade 90/130 is less than in the modified samples with the addition of sulfur. It is observed that the penetration depth increases with increasing sulfur concentration (10%, 30% and 50% of bitumen mass). This indicates an increase in the plasticity and softening of the material with increasing penetration, indicating a decrease in its brittleness. The experimental data in Figure 3 indicates that the effect of sulfur, which has a melting point of 120°C, becomes more prominent as the operating or testing temperature increases, which is consistent with the pattern of increasing its effect on material properties.

In order to determine the viscosity more accurately, we conducted an experiment at 100 g and the results are shown in Figure 4. The analysis of the obtained data shows that when increasing the temperature of sulfur-bitumen binder and increasing the additional load there is a slight increase in the depth of penetration of the needle into the bitumen. Consequently, we can conclude that the additional external load practically does not affect the increase in viscosity of bitumen 90/130 before and after modification with sulfur. It is worth noting that with increasing temperature in the range from 30°C - 50 °C penetration depth increases sharply, which indicates increased plasticity properties of pure and modified bitumen 90/130.

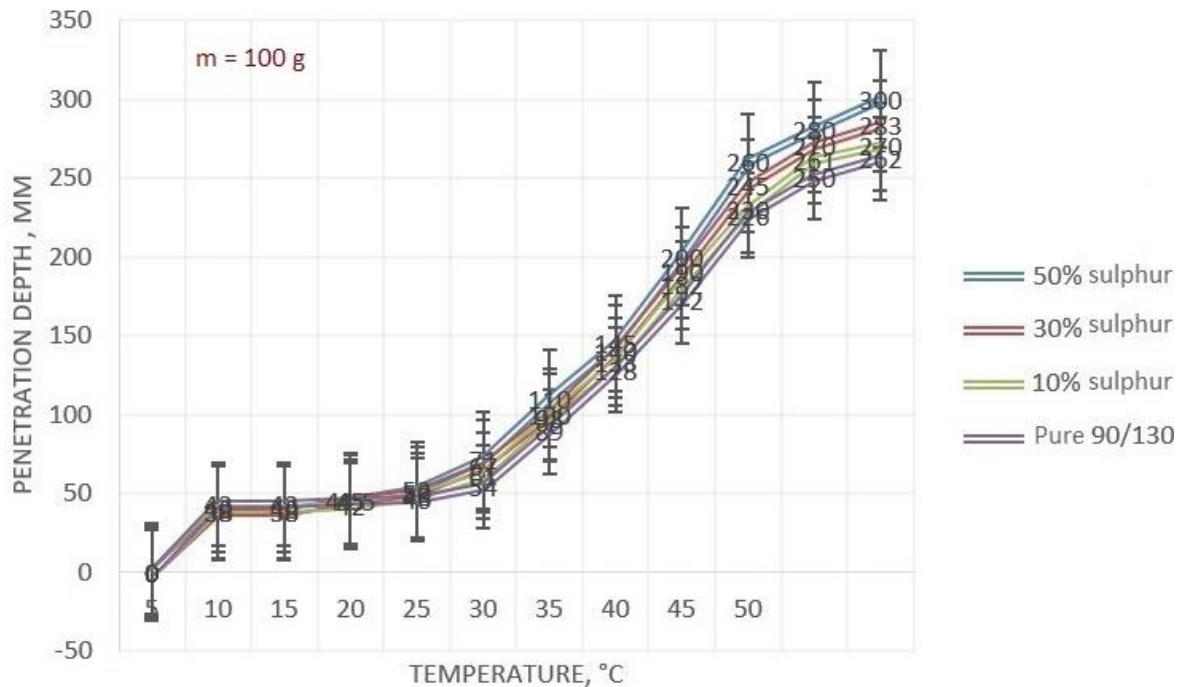


Figure 4 – Dependence of penetration depth on temperature of bitumen 90/130 before and after modification with additional mass of 100 g

#### 4. Conclusions

In this work were investigated physical-mechanical and performance indicators of bituminous binder 90/130 before and after modification with sulfur in proportions of 10%, 30% and 50% of the binder weight. At elemental analysis of spectra of sulfur-modified bitumen binder samples no noticeable chemical changes were revealed. Increasing the mass fraction of sulfur from 10% to 50% in the binder bitumen 90/130 did not lead to the formation of new chemical compounds, which is confirmed by new characteristic peaks. Note that the positions of the main maxima of the recorded spectra did not differ significantly.

Analysis and experimental comparison of softening temperature allowed to reveal insignificant influence of liquid heating rate from the concentration of modifying component. Increase of sulfur concentration more than 10% in the modified bitumen leads to an increase in softening temperature. This is explained by an increase in the amount of sulfur in the system, which causes the formation of a denser structure and an increase in the viscosity of bitumen.

It is revealed that the presence of sulfur as a dispersed phase in bitumen has a regular effect on the mechanical characteristics of sulfur asphalt concretes: there is an increase in mechanical properties with increasing sulfur content.

#### References

1. Method research on evaluation standard of pavement ride quality / X. Zhou, B. Sun, Z. Chen, L. Sun // *Tongji Daxue Xuebao/Journal of Tongji University*. — 2007. — Vol. 35, No. 2. — P. 213–217.
2. Modified binders: an underexploited road maintenance tool / T. Hoban // *Highways Croydon*. — 1987. — Vol. 55, No. 3. — P. 1926.
3. Effect of storage stability on chemical and rheological properties of polymer-modified asphalt binders for road pavement construction / L. Zani, F. Giustozzi, J. Harvey // *Construction and Building Materials*. — 2017. — Vol. 145. — P. 326–335. <https://doi.org/10.1016/j.conbuildmat.2017.04.014>
4. Changes of component and property of pitch road binder modified by rubber during ageing / M.-L. Jin, A.-Z. Feng, M.-R. Shi, X.-G. Chen, C.-Y. Zhang, Y.-H. Li // *Journal of Fuel Chemistry and Technology*. — 2000. — Vol. 28, No. 2. — P. 188.

5. Application of bio-resin in road materials: Rheological and chemical properties of asphalt binder modified by lignin-phenolic resin / Y. Li, C. Lv, P. Cheng, Y. Chen, Z. Zhang // *Case Studies in Construction Materials*. — 2023. — Vol. 18. — P. e01989. <https://doi.org/10.1016/j.cscm.2023.e01989>
6. Assessment of temperature susceptibility for rubber granulate modified road asphalt binders considering impact of aging / M. Słowik, D. Wisniewski, M. Bilski, M. Mielczarek. 2018. — Vol. 222. — P. 01016. <https://doi.org/10.1051/mateconf/201822201016>
7. Casting sulfur pipe / I. Bencowitz // *Industrial and Engineering Chemistry*. — 1938. — Vol. 30, No. 7. — P. 759–764. <https://doi.org/10.1021/ie50343a007>
8. The manufacture of industrial carbons from petroleum raw materials / C.A. Stokes // *Preprints*. — 1975. — Vol. 20, No. 2. — P. 387.
9. Evaluation of Mixture Performance and Structural Capacity of Pavements Using Shell Thiopave / N. Tran, A. Taylor, D. Timm, M. Robbins, B. Powell, R. Dongre // *NCAT Report*. — 2010. — Vol. 10, No. 5. — P. 1597.
10. Field evaluation of sulfur-extended asphalt pavements / T.L. Beatty, K. Dunn, E. Harrigan, K. Stuart, H. Weber // *Transportation Research Record*. — 1987. — Vol. 1115. — P. 116–170.
11. GOST 22245–90 Viscous petroleum road bitumen. — 1991.
12. GOST 127.1-93 Sulphur for industrial use. — 1994.
13. *The Infrared Spectra of Complex Molecules*. — Berlin, Germany: Springer Dordrecht, 1980. — 300 p. <https://doi.org/10.1007/978-94-011-6520-4>
14. Structure Formation and Phase Composition of Sulfur-Bitumen Systems / V. Gladkikh, E. Korolev, D. Husid // *Materials Science Forum*. — 2016. — Vol. 871. — P. 110–117. <https://doi.org/10.4028/www.scientific.net/MSF.871.110>
15. Examination of bitumen-polymers interaction / D.A. Ayupov, L.I. Potapova, A.V. Murafa, V.H. Fakhrutdinova, Yu.N. Khakimullin, V.G. Khozin // *News of Kazan State University of Architecture and Construction*. — 2011. — Vol. 15. — P. 140–145.
16. EN 1426:2015 Bitumen and bituminous binders — 2015.

#### **Information about authors:**

*Tomiris Beisenbayeva* – Master Student, School of Engineering and Digital Sciences, Nazarbayev University, 53 Kabanbay ave., Astana, Kazakhstan, [tbeisenbayeva@mail.ru](mailto:tbeisenbayeva@mail.ru)

*Anna Schmidt* – Master Student, Faculty of Mechanical engineering, University of Applied Sciences Duesseldorf, 156 Münsterstraße st., Duesseldorf, Germany, [as0041526@gmail.com](mailto:as0041526@gmail.com)

#### **Author Contributions:**

*Tomiris Beisenbayeva* – concept, methodology, resources, data collection, testing.

*Anna Schmidt* – modeling, analysis, visualization, interpretation, drafting, editing, funding acquisition.

*Received: 02.10.2023*

*Revised: 23.10.2023*

*Accepted: 23.10.2023*

*Published: 25.10.2023*